

A Parallel Product-Convolution approach for representing the depth Point Spread Function in 3D widefield microscopy based on principal component analysis

Muthuvel Arigovindan^{1*}, Joshua Shaevitz², John McGowan¹, John W. Sedat¹ and David A. Agard^{1†}

¹Keck Advanced Microscopy Center and the Dept. of Biochem. and Biophys., University of California at San Francisco, San Francisco, CA-94158

[†]Howard Hughes Medical Institute

²Department of Physics and Lewis-Sigler Institute for Integrative Genomics, Princeton University, Princeton, NJ-08544

*mvel@msg.ucsf.edu

Abstract: We address the problem of computational representation of image formation in 3D widefield fluorescence microscopy with depth varying spherical aberrations. We first represent 3D depth-dependent point spread functions (PSFs) as a weighted sum of basis functions that are obtained by principal component analysis (PCA) of experimental data. This representation is then used to derive an approximating structure that compactly expresses the depth *variant* response as a sum of few depth *invariant* convolutions pre-multiplied by a set of 1D depth functions, where the convolving functions are the PCA-derived basis functions. The model offers an efficient and convenient trade-off between complexity and accuracy. For a given number of approximating PSFs, the proposed method results in a much better accuracy than the strata based approximation scheme that is currently used in the literature. In addition to yielding better accuracy, the proposed methods automatically eliminate the noise in the measured PSFs.

© 2010 Optical Society of America

References and links

1. D. Agard, Y. Hiraoka, P. Shaw, and J. Sedat, "Fluorescence microscopy in three dimensions", *Methods Cell Biol.* 30, 353–377 (1989).
2. P. Sarder, and A. Nehorai, "Deconvolution methods for 3-D fluorescence microscopy images", *IEEE Sig. proc. mag.* 23, 32–45 (2006).
3. S. Gibson, and F. Lanni, "Experimental test of an analytical model of aberration in an oil-immersion objective lens used in three-dimensional light microscopy". *J. Opt. Soc. Am. A* 8, 1601–1613 (1991).
4. B. Hanser, M. Gustafsson, D. Agard, and J. Sedat, "Phase-retrieved pupil functions in wide-field fluorescent microscopy", *J. Microscopy* 216, 32–48 (2004).
5. J. Shaevitz, and D. Fletcher, "Enhanced three-dimensional deconvolution microscopy using a measured depth-varying point-spread function", *J. Opt. Soc. Am. A* 24, 2622–2627 (2007).
6. C. Preza, and J. Conchello, "Image estimation account for point-spread function depth variation in three-dimensional fluorescence microscopy", *Proc. SPIE*, (2003), pp. 1–8.
7. C. Preza, and J. Conchello, "Depth-variant maximum likelihood restoration for three-dimensional fluorescence microscopy", *J. Opt. Soc. Am. A* 21, 1593–1601 (2004).

8. E. Hom, F. Marchis, T. Lee, S. Haase, D. Agard, and J. Sedat, "AIDA: an adaptive image deconvolution algorithm with application to multi-frame and three-dimensional data", *J. Opt. Soc. Am. A* 24, 1580-1600 (2007).
 9. C. Vonesch, and M. Unser, "A Fast Thresholded Landweber Algorithm for Wavelet-Regularized Multidimensional Deconvolution", *IEEE Tran. Imag. Proc.* 17, 539-549 (2008).
 10. C. Vonesch, and M. Unser, "A Fast Multilevel Algorithm for Wavelet-Regularized Image Restoration", *IEEE Tran. Imag. Proc.* 18, 509-523 (2009)
 11. I. Jolliffe, *Principal component analysis* (Springer, 2002).
 12. S. Wiersma, P. Torok, T. Visser, and P. Varga, "Comparison of different theories for focusing through a plane interface", *J. Opt. Soc. Am. B* 14, 1482-1490 (1997).
-

OCIS codes: 110.0110, 110.0180, 110.6880

1. Introduction

Deconvolution plays a crucial role in 3D wide-field microscopy [1]. It attempts to estimate the underlying image structure from the acquired data by inverting the imaging response (forward model) of the microscope, which leads to an improved resolution and contrast. Undeniably, accuracy of the forward model has a significant impact on the accuracy of the estimated structure. In the standard space-invariant assumption, the forward model is represented by a point spread function (PSF) which is the image resulting from placing a point source (sub-diffraction fluorescent bead) under the microscope. Most of the deconvolution methods rely on this assumption [2]. However, in reality, this assumption is invalid.

In any realistic widefield microscope with high NA objective lens observing biological samples, the actual PSF varies as a function of depth from the coverslip. The dominant factor causing this variation is the depth dependent spherical aberration resulting from the mismatch between the refractive indices of mounting and immersion mediums [3]. Hence, if $N_x \times N_y \times N_z$ is the image size with N_z being the axial dimension, then a rigorous representation amounts to using an N_z number of 3D depth-varying PSFs (DV-PSFs). For a particular imaging set-up, if one has measured the PSF at zero depth, all DV-PSFs are predictable with a reasonable approximation by modifying the phase-retrieved pupil function [4]. It can also be measured with sufficiently fine sampling using specialized hardware [5].

Observation of such PSFs indicate that the magnitude of depth variation is significant, suggesting that including depth-dependent effects in deconvolution will lead to a substantial improvement in the results. This has indeed been demonstrated experimentally in [5] where both the data and PSFs used were from real measurements. The emphasis therein was on showing the advantage in using the depth variant forward model against the invariant one, but not on the computational complexity. Since, it is impractical to use N_z number of PSFs, the authors use an approximation method where the depth-dependent effects are handled as discrete layers or strata in Z (strata method) [6, 7].

It should be noted that most of the high performance nonlinear deconvolution methods [8, 9, 10] rely on repeated computation of the forward model. Hence, an improved approximation method will result in a significant improvement in the deconvolution process.

Our goal in this paper is to develop a better approximation scheme based on principal component analysis. We restrict ourselves in developing the forward model only and we do not consider the deconvolution problem here. With the use of theoretical and measured PSFs, we demonstrate how our model provides a better alternative for constructing deconvolution algorithms.

2. Developing the model

Our model is based on expressing the DV-PSFs as weighted sum of a fixed set of basis functions derived from the the principal components of experimental observations. Since, PCA of 3D images is extremely complex and computationally impractical (with no reported applications so far), we first derive an approximate two-stage method, which we call the tensor product PCA (TP-PCA). We then derive the final computational structure. Thus, the depth variation is accounted for by premultiplication with a set of 1D depth functions, followed by a set of standard convolutions.

2.1. Tensor product PCA of 3D images

Principal component analysis [11] allows a compact representation of images of a given specific class. It represents a given set of images as a weighted sum of a small number of 2D basis functions, These basis functions are known as the principal components which are computed using Singular Value Decomposition (SVD) as described below.

Let $\{\mathbf{X}_1, \mathbf{X}_2, \dots, \mathbf{X}_N\}$ be the given set of images. Let $\bar{\mathbf{X}}$ be the mean image given by

$$\bar{\mathbf{X}} = (1/N) \sum_{i=1}^N \mathbf{X}_i.$$

Let \mathbf{v}_i be the 1D vector obtained by scanning the mean removed image $\mathbf{X}'_i = \mathbf{X}_i - \bar{\mathbf{X}}$. Let \mathbf{R} be the matrix defined by

$$\mathbf{R} = [\mathbf{v}_1 \ \mathbf{v}_2 \ \dots \ \mathbf{v}_N]$$

\mathbf{R} is an $M \times N$ matrix where M is the total number of pixels in each of the images $\{\mathbf{X}_1, \mathbf{X}_2, \dots, \mathbf{X}_N\}$. Let the following be the singular value decomposition of \mathbf{R} .

$$\mathbf{R} = \mathbf{U}\mathbf{D}\mathbf{V}^T,$$

where \mathbf{U} and \mathbf{V} are orthogonal matrices and \mathbf{D} is a diagonal matrix. Without the loss of generality, let us assume that the diagonal elements of \mathbf{D} are ordered with decreasing magnitude. Let \mathbf{u}_i be the i th column of \mathbf{U} , and \mathbf{P}_i be the corresponding image obtained by reverse scanning \mathbf{u}_i . Then in PCA, one choses the first B column vectors of \mathbf{U} and expresses an input image \mathbf{X}_i as

$$\mathbf{X}_i = \bar{\mathbf{X}} + \sum_{j=1}^B c_{i,j} \mathbf{P}_j,$$

where $c_{i,j} = \langle \mathbf{P}_j, \mathbf{X}'_i \rangle$, with $\langle \cdot, \cdot \rangle$ representing the inner product, i.e., point-wise multiplication and summation. The user-defined parameter, B , in the above expression represents the number of basis functions, which is chosen according to the required level of approximation. The diagonal elements of \mathbf{D} provide an estimate of approximation error. Specifically, the ratio,

$$r_B = \frac{d_B}{d_1},$$

gives relative mean square approximation error, where the d_i s represent the diagonal elements of \mathbf{D} . Typically, for an adequate level of approximation, B is much smaller than N .

Almost all of the imaging applications that use PCA are on 2D images. A direct application of the above procedure is impractical for 3D images because SVD becomes prohibitively expensive. Here we develop a novel two-stage method, which we call the tensor product PCA (TP-PCA) that can be applied to the 3D PSF images with an affordable complexity.

Let $\mathcal{S} = \{\mathbf{S}_1(x, y, z), \dots, \mathbf{S}_N(x, y, z)\}$ be the set of 3D images. Let N_z be the number of z sections. For each value of z , we form a set of 2D images given by $\mathcal{S}^{(z)} = \{\mathbf{S}_1^{(z)}(x, y), \dots, \mathbf{S}_N^{(z)}(x, y)\}$, where $\mathbf{S}_i^{(z)}(x, y) = \mathbf{S}_i(x, y, z)$. We then apply PCA on each of the subsets to get basis functions $\mathbf{P}_1^{(z)}(x, y), \dots, \mathbf{P}_{B_1}^{(z)}(x, y)$, where B_1 is a user parameter. The images are expressed as

$$\mathbf{S}_i^{(z)}(x, y) = \bar{\mathbf{S}}^{(z)}(x, y) + \sum_{j=1}^{B_1} c_{i,j}^{(z)} \mathbf{P}_j^{(z)}(x, y), \quad (1)$$

where $\bar{\mathbf{S}}^{(z)}(x, y)$ is the mean image of the set $\mathcal{S}^{(z)}$ and

$$c_{i,j}^{(z)} = \left\langle \mathbf{S}_i^{(z)}(x, y) - \bar{\mathbf{S}}^{(z)}(x, y), \mathbf{P}_j^{(z)}(x, y) \right\rangle.$$

We now form a set of 2D images given by

$$\mathcal{S}' = \left\{ C_i(z, j) = c_{i,j}^{(z)}, i = 1, \dots, N; j = 1, \dots, B_1 \right\}. \quad (2)$$

Finally, we apply a PCA again on the set \mathcal{S}' to get basis functions $\mathbf{P}'_1(z, j), \dots, \mathbf{P}'_{B_2}(z, j)$, where B_2 is the second user parameter. The images are approximated as

$$C_i(z, j) = \sum_{k=1}^{B_2} c'_{i,k} \mathbf{P}'_k(z, j), \quad (3)$$

where $c'_{i,k} = \langle C_i(z, j), \mathbf{P}'_k(z, j) \rangle$. Substituting (3) and (2) in (1) gives

$$\mathbf{S}_i^{(z)}(x, y) = \bar{\mathbf{S}}^{(z)}(x, y) + \sum_{k=1}^{B_2} c'_{i,k} \mathbf{Q}_k(x, y, z),$$

where

$$\mathbf{Q}_k(x, y, z) = \sum_{j=1}^{B_1} \mathbf{P}'_k(z, j) \mathbf{P}_j^{(z)}(x, y)$$

Replacing $\mathbf{S}_i^{(z)}(x, y)$ and $\bar{\mathbf{S}}^{(z)}(x, y)$ by $\mathbf{S}_i(x, y, z)$ and $\bar{\mathbf{S}}(x, y, z)$ in (2.1) yields

$$\mathbf{S}_i(x, y, z) = \bar{\mathbf{S}}(x, y, z) + \sum_{k=1}^{B_2} c'_{i,k} \mathbf{Q}_k(x, y, z), \quad (4)$$

The above expression represents our final TP-PCA approximation. In the above procedure, the first user parameter B_1 is chosen such that the approximation error is negligible or zero in the first stage, and the second user parameter is chosen according to the desired final approximation error. By this way, the overall approximation error is governed only by the z -dependent second stage.

We have described so far a procedure that gives orthogonal basis functions for 3D images by performing $N_z + 1$ 2D PCA decompositions. Even though the resulting basis functions are not as optimal as the ones that might be obtained by direct 3D PCA (the impractical method), we will show experimentally that this approach works well for approximating 3D PSFs.

2.2. The PCA based imaging model

We are now ready to derive the Parallel Product-Convolution structure. Consider the scheme represented in the Figure 1(a). The fluorescent object to be studied is mounted under a coverslip and placed below the objective lens. The space between the objective lens and the coverslip is filled with the immersion medium (oil) whose refractive index matches with that of the coverslip. The refractive index of the object differs from that of the coverslip and oil, and is typically assumed to be uniform. In essence, there is only one discontinuity along the optical axis that is represented by a plane, which results in the depth varying response of the system.

Typical 3D imaging involves acquiring a series of 2D images for different values of z or equivalently different positions of the focal plane (Figure 1(a)). Note that z represents the position of the focal plane with respect to the interface plane. If there is no refractive index mismatch, the 3D image is expressed in terms of the object by a simple convolution with a 3D PSF. However, to express the image in terms of the object under the coverslip when there is a mismatch, we need the 4D function, $h'(x, y, z, z')$, which represents the series of 2D image resulting from positioning the focal plane at z and a point source at z' (Figure 1(b)).

Let $f(x, y, z)$ be the object (fluorescent dye structure) and $g(x, y, z)$ be the image acquired by the microscope. The forward model is given by

$$g(x, y, z) = \int_{x', y', z'} h'(x - x', y - y', z, z') f(x', y', z') dx' dy' dz', \quad (5)$$

In the above expression, z is the axial image coordinate and z' is the axial object coordinate and the system response is a function of both.

Under this notion, when the system is depth independent, the response is a function of only the difference $z - z'$. In other words, the depth invariance corresponds to following relation:

$$h'(x, y, z, z') = h'(x, y, z - z', 0),$$

and (5) becomes a simple convolution given by

$$g(x, y, z) = h_0(x, y, z) * f(x, y, z),$$

where $h_0(x, y, z)$ is the standard depth independent PSF given by $h_0(x, y, z) = h'(x, y, z, 0)$.

The next step is to account for the focus shift [12] in the representation of h' . The term focus shift signifies the fact that, for a given value of object depth variable z' , the maximum intensity is observed when the image depth variable z is equal to az' , where a is a constant that depends on the refractive indices of the mounting and immersion mediums. To account for the focus shift, we consider the followed transformation (Figure 1(c)):

$$h(x, y, z, z') = h'(x, y, z + az', z'). \quad (6)$$

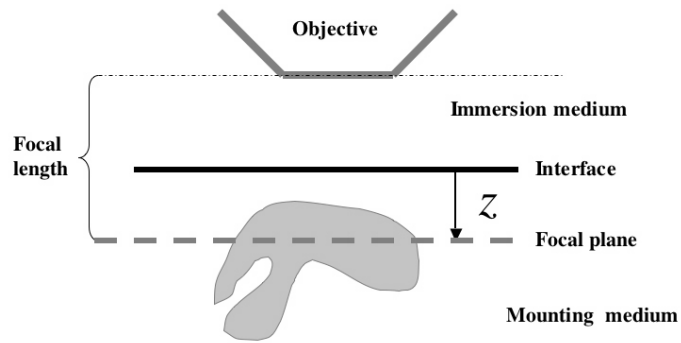
Note that now in the new representation, the reference plane for z is the plane containing the bead with focus shift. This representation is advantageous in the sense that, for a fixed value of x, y , and z , the variation with respect to axial object coordinate z' is lower compared to the former representation.

The forward model with new representation becomes

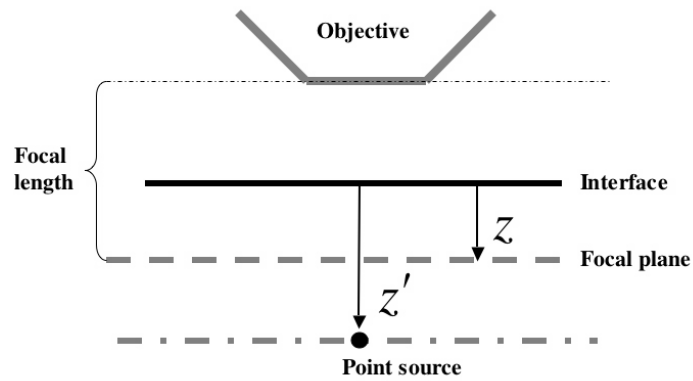
$$g(x, y, z) = \int_{x', y', z'} h(x - x', y - y', z - az', z') f(x', y', z') dx' dy' dz',$$

The above equation can be equivalently represented by

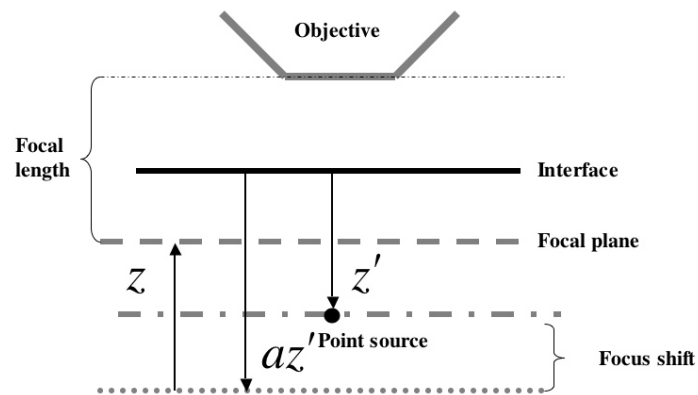
$$g(x, y, z/a) = \int_{x', y', z'} h(x - x', y - y', z/a - z', z') f(x', y', z') dx' dy' dz',$$



(a) Schematic of 3D acquisition



(b) Axial variables of h'



(c) Axial variables of h (eqn. (6))

Fig. 1. Schematic representation 3D depth dependent system

The factor a in the above expression disappears if it is translated into discrete summations assuming that discretization step size of z is a times larger than that of z' . Assuming now that the variables represent discrete indices, the above model becomes

$$g(x, y, z) = \sum_{x', y', z'} h(x - x', y - y', z - z', z') f(x', y', z'), \quad (7)$$

Now, define the set of 3D images given by

$$\mathcal{S} = \{h_{z'}(x, y, z) = h(x, y, z, z'), z' = 0, \dots, N_z - 1\}$$

We then apply a TP-PCA as described in the previous subsection. Let $P_1(x, y, z), \dots, P_B(x, y, z)$ be the selected principal components¹. Then, the function $h(\cdot, \cdot, \cdot, \cdot)$ can be approximated as

$$h(x, y, z, z') = \bar{h}(x, y, z) + \sum_{j=1}^B c_j(z') P_j(x, y, z), \quad (8)$$

where $\bar{h}(x, y, z)$ is the function obtained by averaging $h(x, y, z, z')$ along z' , and

$$c_j(z') = \sum_{x, y, z} (h(x, y, z, z') - \bar{h}(x, y, z)) P_j(x, y, z)$$

Substituting (8) in (7) yields the final structure:

$$g(x, y, z) = \bar{h}(x, y, z) * f(x, y, z) + \sum_{j=1}^B P_j(x, y, z) * [c_j(z) f(x, y, z)], \quad (9)$$

where $*$ represents convolution. The equation (9) is our parallel product-convolution (PPC) model. The complicated integral (5) is approximated by simple expression (9) involving a set of standard convolutions with the input pre-multiplied by 1D functions. The above approximation model can be re-expressed as in the equation (5) with h replaced by $h_a^{(B)}$, where the latter is given by

$$h_a^{(B)}(x, y, z, z') = \bar{h}(x, y, z) + \sum_{j=1}^B P_j(x, y, z) c_j(z'). \quad (10)$$

Let $N_x \times N_y \times N_z$ be the image size. A quick examination of (9) might indicate that its implementation will require $B + 1$ number of 3D FFTs and a 3D IFFT. However, observing the fact that input to $B + 1$ convolutions differ only axially, it can be verified that $B + 1$ number of 3D FFTs can be replaced by N_z times 2D FFTs and then $(B + 1)N_x N_y$ times 1D FFTs, providing additional computational efficiency.

3. Results

We apply our method on both theoretical and measured PSFs and compare with the bilinear interpolation method reported in [7]. In this method, the z' -axis is divided into some number of intervals (strata) of thickness T and the DV-PSFs at the edge of the intervals are used to approximate all the DV-PSFs using bilinear interpolation.

We used the same experimental set-up as in [5] to obtain measured DV-PSFs. DV-PSFs were measured by positioning fluorescent beads at various depths (z') using an optical trap (refer to [5] for experimental set up). Imaging wavelength was 532 nm. The discretization step size for x

¹With reference to the notation in the previous subsection (eqn. (4)), these functions should be $Q_1(x, y, z), \dots, Q_{B_2}(x, y, z)$. We use the current notation for convenience.

and y was 42 nm and that of z' was 75 nm. z step size was chosen appropriately to compensate for the focus shift. The objective numerical aperture was 1.49 NA. We also used the same specifications to generate theoretical DV-PSFs using the method described in [4].

To visualize the DV-PSFs we utilize both xz sections for various values z' with y chosen to be at the center of the PSFs, and xz' sections for various values z with y chosen similarly. In all the visualizations, the top left corner corresponds to the origin of the axes. To make low intensities visible, we display the fourth root of the intensity whenever the images are positive. The exceptions are the approximation error images, and the PCA basis functions.

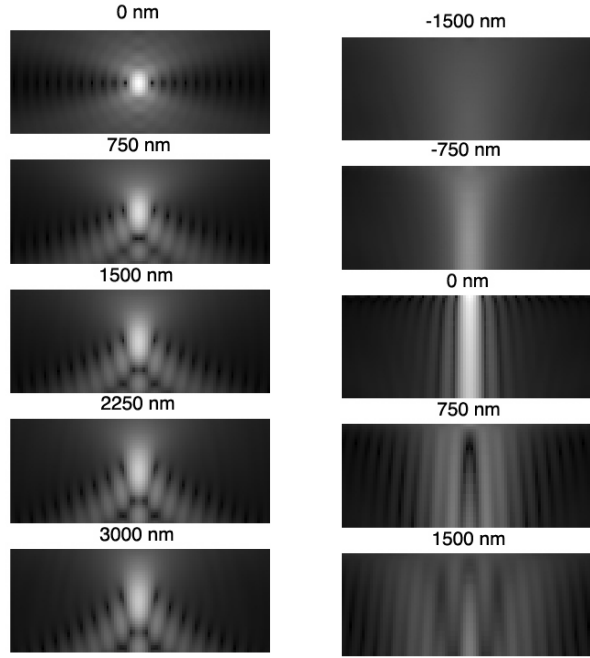
For a given B , we define the normalized approximation error as

$$E = \frac{\|h - h_a^{(B)}\|^2}{\|h\|^2},$$

where $h_a^{(B)}$ is as defined in (10).

3.1. Application to theoretical PSFs

We used 41 theoretical 3D PSFs of size $100 \times 100 \times 40$ for $\{z' = i \times 75 \text{ nm}, i = 0, \dots, 40\}$. Figure 2 displays the xz and xz' sections and Figure 3 shows few first PCA basis functions.



(a) xz section for various values of z' (b) xz' sections for various values of z

Fig. 2. Theoretical DV-PSF sections. Horizontal axis represent x . Image size is $2925 \text{ nm} \times 4200 \text{ nm}$.

Figure 4 compares the approximation error for fitting a set of 41 3D PSFs using either the PCA method or the strata based method given in [7] for various number of PSF basis functions. Note that the basis PSFs for the strata method are selected from the DV-PSFs themselves,

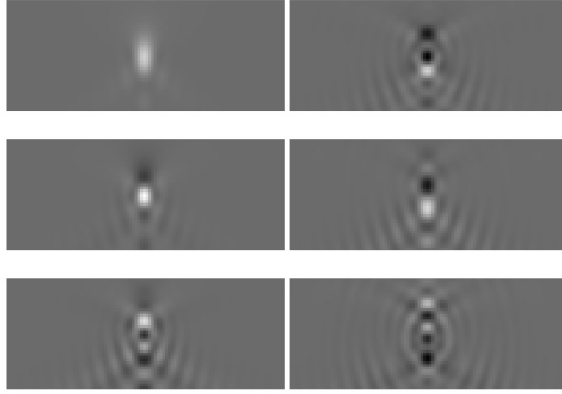


Fig. 3. Basis functions for theoretical PSFs (xz sections). Image at the top left is the mean PSF \bar{h} . The remaining are the first 5 principal components.

whereas for our method, the basis PSF functions are the mean PSF and the principal components. The advantage of using the PCA method over the strata method is evident from the plot; 2 PCA functions outperform 5 strata functions and 3 PCA functions are comparable to 8 strata functions.

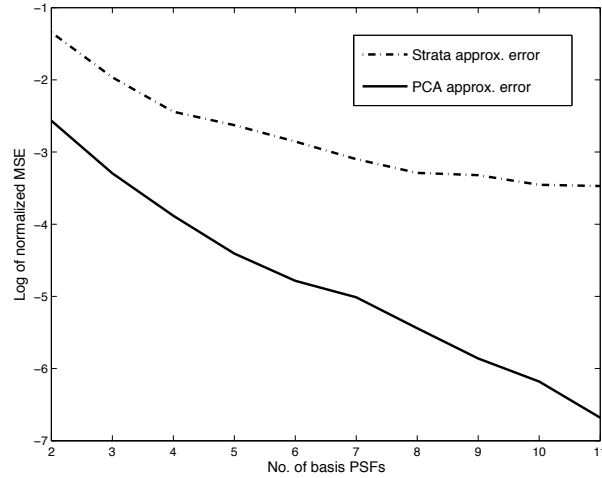


Fig. 4. Approximation error for various values of number of basis PSFs. x -axis represents number of PSFs used to approximate 41 PSFs spanning the range $z' = [0, 3000 \text{ nm}]$. PCA method yields a significant advantage over the strata based method.

We now consider the special case of approximating the DV-PSFs with two bases PSFs. This amounts to, for PCA method, using the mean PSFs \bar{h} and the first principal component; whereas, for the strata method, this means using the PSF corresponding to values of z' equal to zero and bottom of the total range. Figure 5 compares the approximated PSFs with the originals for both methods. In the strata method, for the PSFs at the top and the bottom, the approximated PSFs are identical to the originals since these PSFs are themselves the basis functions. However, for

the total range of z' , the mean approximation error is much higher than that of PCA method (about 17 times). This is evident from the approximated images in the middle (for $z' = 750$ nm, 1500 nm, 2250 nm). Figure 6 shows the xz' sections of the same results. While visually less obvious, comparable behavior extends to any number of basis functions.

3.2. Application to measured PSFs

We used a set of 41 measured 3D PSFs obtained using the set-up described at the beginning of this section. The results are analogous to that of the previous subsection; the only difference is that the PSFs used here are real measured PSFs. Figure 7 displays the xz and xz' sections and Figure 8 shows first two PCA basis functions. We observed that, subsequent basis functions contain background noise as well as high frequency structures that lie well beyond the theoretical frequency support of the microscope, which possibly originate from the Poisson noise. This indicates that two bases function are sufficient to represent the essential details of DV-PSFs for the range of depth considered in this experiment.

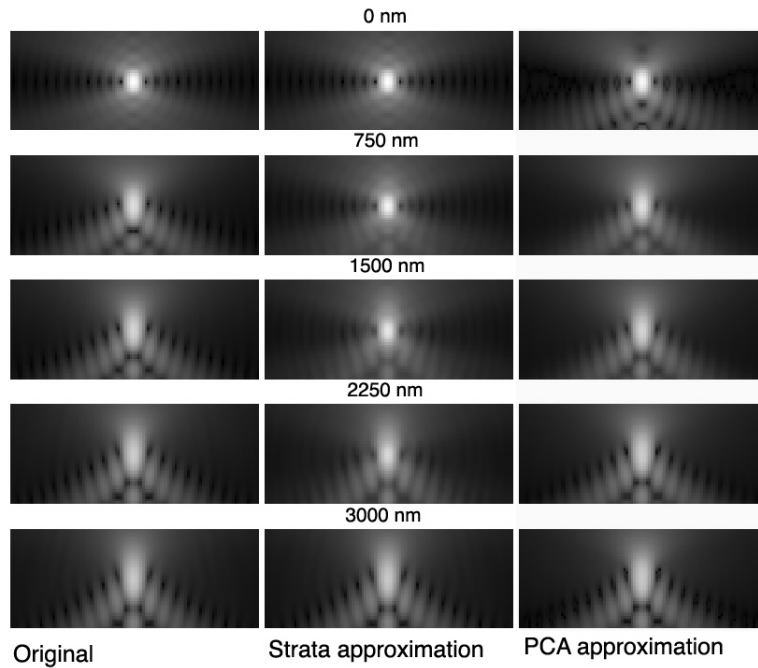
Figure 9 compares the approximation error of the PCA method with that of the strata based method for various number of bases PSFs. As with the theoretical PSFs, the PCA method provides an improved approximation. However, the error does not fall off as fast as in the case of theoretical PSF approximation, since the measured PSFs contain noise.

We now again consider the special case of approximating the DV-PSFs with two basis PSFs. Figure 11 displays the results. It should be noted that, for the strata method, the calculated PSFs at the top and the bottom are identical to the originals (including the background noise) since these PSFs are themselves used as the basis functions. Whereas, in PCA method, the approximations differ from the original both in terms of the noise and signal for these two values of z' . However, for the other values of z' , the PCA method yields a smaller error, and all of the approximated PSFs are nearly noise-free. This result is also evident from the displayed error images (Figure 11(b)). In contrast to the case of theoretical PSFs, here the PCA method provides only a two fold improvement in the error, due to the inclusion noise. Figure 10 displays the xz' section of the same result for $z = 0$. We can see significant line artifacts in the strata approximated PSFs which originates from interpolated noise.

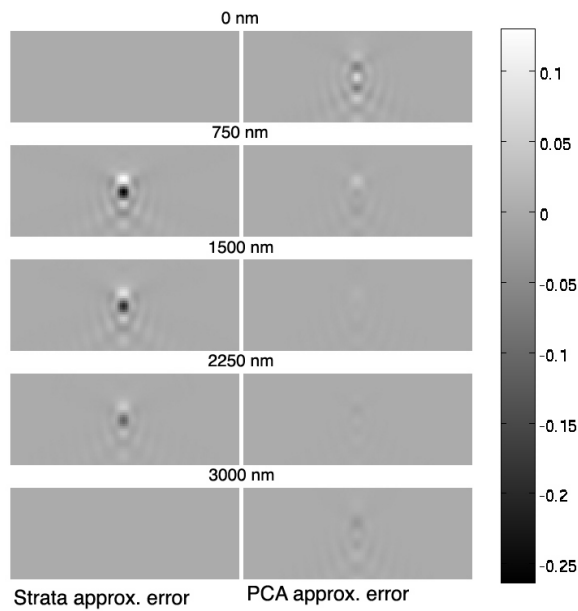
Based on the above experimental observations, we now summarize the factors that render the proposed method an attractive tool for constructing robust depth dependent deconvolution algorithms. We first note that a robust deconvolution method typically uses a nonquadratic regularization. It computes the required solution as a minimizer of a weighted sum of this regularization and a quadratic data fidelity term [8, 9, 10]. Such algorithms typically take about 300 seconds for computing a 3D stack of standard size. If these algorithms are extended for depth dependent deconvolution, the computational time will be multiplied by a factor proportional to the number of PSFs used. Hence using a large number of PSFs is not practical. Since the proposed method approximates the DV-PSFs with a very few basis PSFs, it will be a promising tool for solving depth dependent deconvolution problems using general purpose computers with a moderate computational power. For example, a 5 PSF model, which approximates both experimental and theoretical PSFs with more than 95% accuracy, offers a good trade-off between computational complexity and accuracy.

Second, for a given number of basis PSFs, the proposed method has a lower computational complexity than that of the strata method as explained at the end of section 2. For example, when a 5-PSF model is used, the strata method will cause a 5 fold increase in the computational complexity when compared to depth invariant deconvolution, whereas the proposed method will cause only about a 3 fold increase. This gain originates from the compactness of the forward model expressed in the equation (9).

Another interesting point is that, since the proposed model automatically eliminates noise

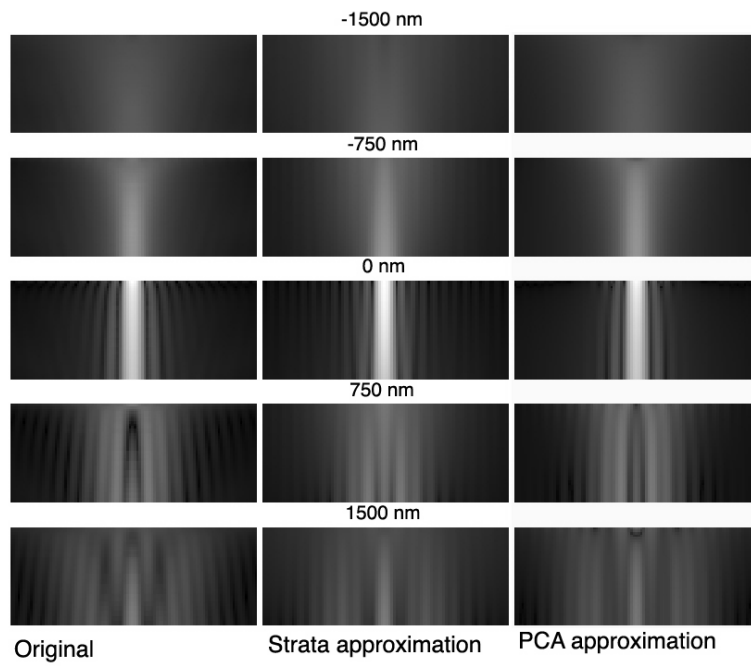


(a) Approximated xz sections

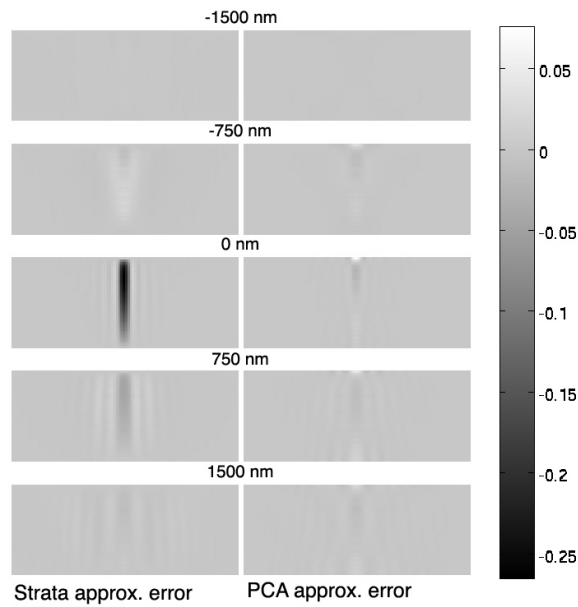


(b) xz sections of normalized approximation error

Fig. 5. Results of approximating using two basis functions only. Displayed are the approximated xz sections and error images for various values of z' . For $z' = 0$ nm, 3000 nm, strata approximation is identical to the originals because the basis function therein are originals themselves. However, for the other values of z' , PCA method gives better approximation resulting in a 17 fold improvement in overall approximation error. The displayed error images are normalized to the overall maximum of the original PSFs.

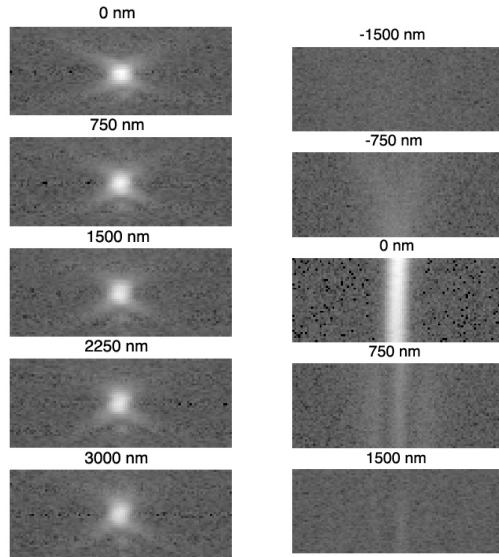


(a) Approximated xz' sections



(b) xz' sections of normalized approximation error

Fig. 6. xz' sections of the same results in Figure 5 for various values of z



(a) xz section for various values of z (b) xz' sections for various values of z

Fig. 7. Measured DV-PSF sections. Image size is $2925\text{nm} \times 4200\text{nm}$.



Fig. 8. Basis functions for measured PSFs (xz sections). Image at the left is the mean PSF \bar{h} . The right one is the first principal component.

without losing low intensity features in the DV-PSFs, the PCA-approach will reduce the potential for artifacts in the deconvolution results.

4. Conclusions

We have developed a PCA based approximation model for use in deconvolving the depth varying response of widefield microscopes. When compared to the only available method in literature, namely the strata based interpolation method, the PCA method results in a much lower approximation error for any given number of model PSFs. Simultaneously, the PCA method automatically eliminates the noise in the measured PSFs, in contrast to the strata based method. Using this new model in any iterative deconvolution algorithm is thus expected to result in a greatly improved restoration of biological structures.

Acknowledgements

This research was supported by Human Frontiers Science Program Organization (www.hfsp.org) under the grant LT00460/2007-C.

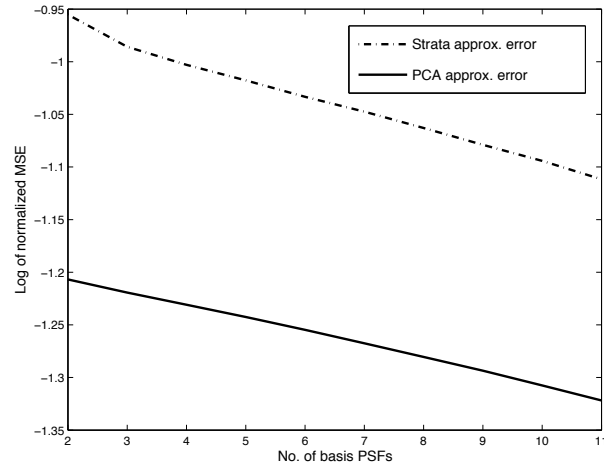


Fig. 9. Approximation error for various values of number of basis PSFs. x -axis represents number of PSFs used to approximate 41 PSFs spanning the range $z' = [0, 3000 \text{ nm}]$. PCA method yields a better approximation.

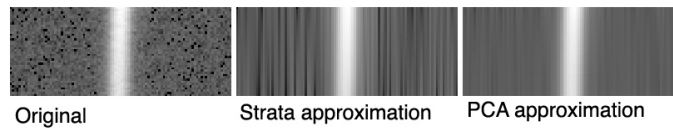
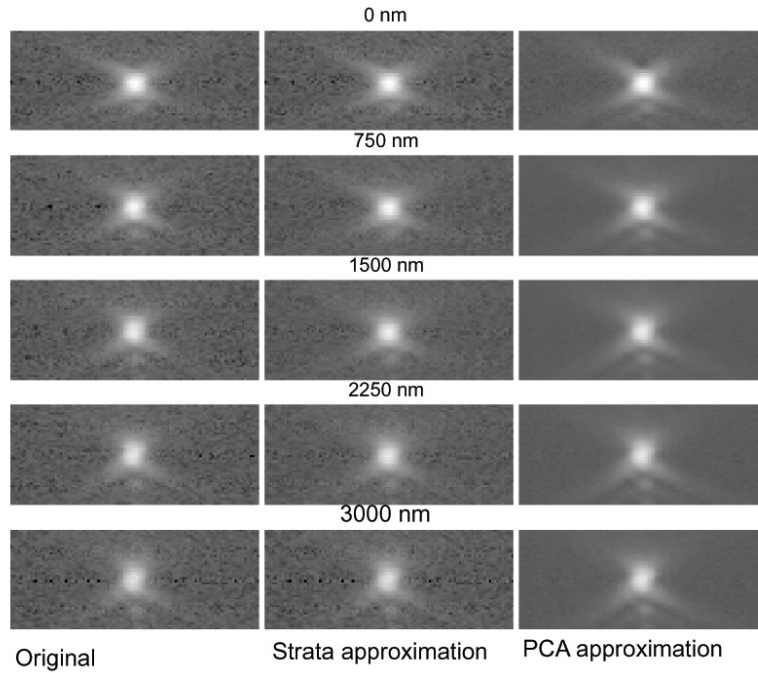
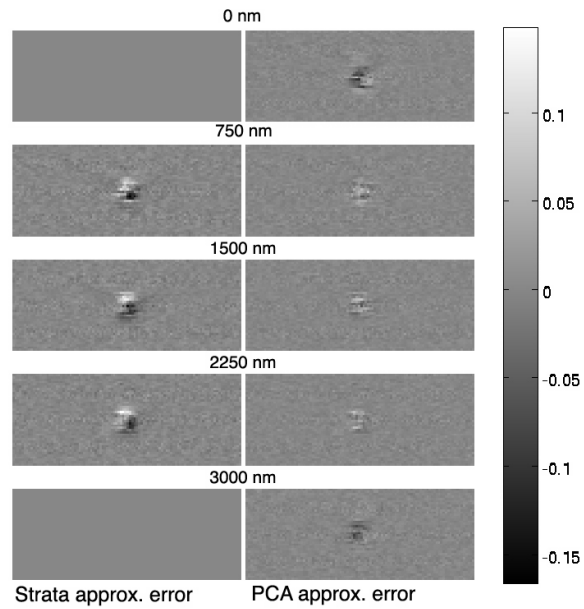


Fig. 10. xz' section of approximation result of Figure 11 for $z = 0$. Note the pronounced line artifact in strata approximation.



(a) Approximated xz sections



(b) xz sections of normalized approximation error

Fig. 11. Results of approximating using two basis functions only. Displayed are the approximated xz sections and error images for various values of z' . For $z' = 0$ nm, 3000 nm, strata approximation is identical to the originals because the basis function therein are originals themselves. However, for the other values of z' , PCA method gives better approximation.